

Observed Impact of the South Asian Summer Monsoon on the Local Meteorology in the Himalayas

ZHOU Libo*(周立波), ZOU Han (邹 捍), MA Shupo (马舒坡), and LI Peng(李 鹏)

LAPC, Institute of Atmospheric Physics, Chinese Academy of Sciences, Beijing 100029

(Received July 4, 2011; in final form November 16, 2011)

ABSTRACT

The South Asian summer monsoon (SASM) is the most important climate system in Asia. Using observational data from the HEST2006 (Himalayan Exchange between the Surface and Troposphere 2006) campaign and large-scale grid data, this paper analyzed the SASM impact on local meteorological parameters including radiation, temperature, humidity, and wind in the Himalayas. The SASM experienced one active and one break period during the HEST2006 campaign. The local meteorological parameters exhibit great differences between the active period and the break period of the SASM. The radiation fluxes are greater in the break period than in the active period. The air temperature and specific humidity are lower, but soil temperature and wind speed are higher in the break period than in the active period. Further analysis indicates that the SASM greatly affects the meteorological features of the Himalayan region.

Key words: the South Asian summer monsoon, the Himalayas, local meteorology

Citation: Zhou Libo, Zou Han, Ma Shupo, et al., 2012: Observed impact of the South Asian summer monsoon on the local meteorology in the Himalayas. *Acta Meteor. Sinica*, **26**(2), 205–215, doi: 10.1007/s13351-012-0206-0.

1. Introduction

As one of the most important climate systems, the South Asian summer monsoon (SASM) greatly influences the atmospheric processes over Asia (e.g., Li and Yanai, 1996; Webster et al., 1998; Hsu et al., 1999; Goswami and Xavier, 2003; Goswami et al., 2003). Examples of the importance of the SASM include the acceleration of lower-level westerly wind in the tropical East Indian Ocean, the seasonal reversal of the tropospheric meridional temperature gradient, and the formation of cyclonic vortices in the Bay of Bengal or the Southeast Arabian Sea (e.g., Lau and Yang, 1997; Matsumoto, 1997; Wang and Lin, 2002; Liu et al., 2002; Zhang et al., 2004; Ding and Liu, 2006). The heavy and light rainfalls associated with the different monsoon troughs over South Asia are usually observed during the active and break periods of the SASM (Krishnamurti and Ardanuy, 1980; Webster et

al., 1998; Krishnamurthy and Shukla, 2000; Ding and Sikka, 2006).

The Tibetan Plateau (TP) is the most important geographic feature of Asia, with its average altitude above 4000 m and an area over 2.3×10^6 km². Strong solar radiation makes the elevated plateau surface a heating source, which drives atmospheric processes (Ye and Gao, 1979). The TP therefore plays important roles in the Asian climate systems (Flohn, 1957; Ye, 1981; Chen et al., 1985; He et al., 1987; Yanai et al., 1992; Li and Yanai, 1996; Wu and Zhang, 1998; Zhang et al., 2004; Yanai and Wu, 2006; Sato and Kimura, 2007). Its heating greatly contributes to the SASM onset by reversing the upper-tropospheric meridional temperature gradient in the southern TP (Yanai and Li, 1994; Li and Yanai, 1996; Wu and Zhang, 1998). On the other hand, the evolution of the SASM itself contributes greatly to the atmospheric circulation, moisture conditions, and precipitation

Supported by the National Basic Research and Development (973) Program of China (2009CB421403), Knowledge Innovation Project of the Chinese Academy of Sciences (KZCX3-YW-Q11-01), Public Science and Technology Research Funds for Projects of Ocean (201005017-5), China Meteorological Administration Special Public Welfare Research Fund (GYHY201206041), and National Natural Science Foundation of China (40905067).

*Corresponding author: zhoulibo@mail.iap.ac.cn.

over the TP (Luo and Yanai, 1983; Chen et al., 1985; He et al., 1987; Zhang et al., 2004; Gao et al., 1985; Yao et al., 2009).

The altitude of Himalayas averages above 6000 m, and the mountain range extends more than 2000 km along the southern edge of the TP and adjacent to the SASM region. The Himalayas forms the border along which the atmospheric systems of the TP and SASM interact most. After the SASM onset, water vapor passes through the Himalayas from the Bay of Bengal to the interior of Tibet (Gao et al., 1985). Both the Himalayan circulation and large-scale monsoon flows greatly affect the diurnal variation of precipitation in the Himalayas during monsoon season (Barros and Lang, 2003). Most recent results suggest that the Himalayas can produce a strong monsoon by insulating warm, moist air over continental India from the cold and dry extratropics (Boos and Kuang, 2010). Studies of the Himalayan meteorological parameters have indicated features of the atmospheric temperature, moisture, and wind conditions in the Khumbu, Kali Gandaki, and Rongbuk valleys (Tartari et al., 1998; Egger et al., 2000, 2002; and Zou et al., 2008). The results revealed that strong up- and down-valley winds existing in the Himalayas could be thermally driven by strong solar radiation. Although Ueno et al. (2008) and Meinke et al. (2007) revealed that the precipitation in the Himalayan Khumbu valley is closely related to the monsoon weather in Nepal, few recent studies have focused on the impacts of the SASM on Himalayan meteorological phenomena, despite the proximity of the mountain range to the SASM.

In June 2006, the HEST2006 (Himalayan Exchange between the Surface and Troposphere 2006) observational campaign was carried out in the Rongbuk valley on the northern slope of Mt. Qomolangma, in which the radiation, temperature, moisture, and circulation were continuously observed within the active and break periods of the SASM. The objectives of the present study are 1) to identify the active and break periods of the SASM during the HEST2006 campaign, during which the synoptic situations exhibit major changes over the South Asian region, 2) to present comprehensively the radiative, thermal, moisture, and wind conditions in the Himalayas corresponding to the

SASM active and break periods, and 3) to discuss the influences of the SASM on Himalayan meteorology.

2. Measurements and observational data

To better understand the air mass/energy exchange processes between surface and air in the Himalayas and their responses to the South Asian summer monsoon, the HEST2006 campaign was carried out in the Rongbuk valley on the northern slope of Mt. Qomolangma by the Chinese Academy of Sciences in June 2006. The star in Fig. 1a denotes the campaign field in the middle Himalayas. Figure 1b shows the topography of the Mt. Qomolangma region with 1000-m elevation intervals. The Rongbuk valley starts from three glaciers on the northern slope of Mt. Qomolangma, i.e., the East, Middle, and West Rongbuk glaciers. It then runs northward with an approximately 20° trend west of due north, turning to the east at the end of the valley. Two other glaciers, the Jiuda and Gezhongkang, are located in the western mountains of the valley. The valley floor, approximately 1000-m wide and 1000-m deep, lies approximately 5000 m above sea level, and is surrounded by mountains reaching over 6500 m in height in the neighboring regions. The valley surface is semiarid and primarily covered by soil, stones of various sizes and scattered small vegetation.

During the HEST2006 campaign, three observation sites were established along the Rongbuk valley from south to north, located at (A) 28.25°N , 86.82°E , 4765 m, (B) 28.17°N , 86.84°E , 5050 m, and (C) 28.13°N , 86.86°E , 5171 m, respectively. The MAWS systems (Vaisala MAWS101) were used at the three sites to measure global and net radiation fluxes, soil and surface air temperatures, relative humidity, pressure, and surface wind speed at 10-min intervals from 1 to 30 June 2006. In addition, a wind profiler (Vaisala LAP3000) was operated at Site B in the middle of the valley to monitor the wind speed from approximately 150 to 2500 m above the ground with a 50-m vertical resolution at 30-min intervals. The wind speed between the surface and 150 m was obtained using a logarithmic interpolation method. The global and net radiation fluxes, soil temperature, surface air tempera-

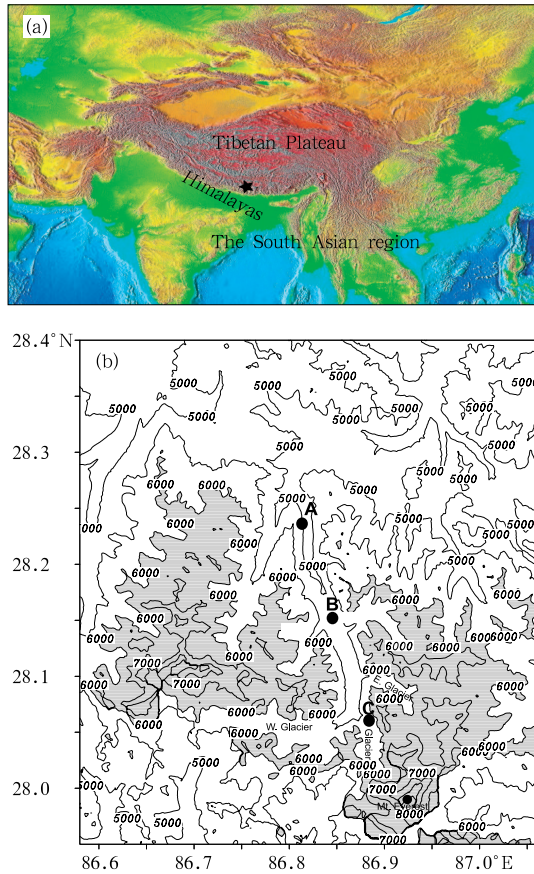


Fig. 1. Topography of the Tibetan Plateau. (a) An overview, with the star denoting approximately the campaign field. (b) The topography of Mt. Qomolangma with 1000-m contour intervals. In (b), shadings denote regions with altitude higher than 6000 m, and the three observation sites A, B, and C are denoted by circles and distributed along the Rongbuk valley from north to south.

ture, and surface specific humidity were averaged over the three sites to represent the local atmospheric properties in the Rongbuk valley.

In addition to the observation data, this study uses the large-scale gridded reanalysis data from the National Centers for Environmental Prediction/National Center for Atmospheric Research (NCEP/NCAR) to calculate average daily quantities at 8-h intervals of the geopotential height, temperature, relative humidity, and wind speed. The data are available at http://www.nomad2.ncep.noaa.gov/ncep_data/. The precipitation data are from the Global Precipitation and Climatology Project (GPCP), available at <ftp://precip.gsfc.nasa.g>

<ov/pub/gpcp-v2/psg>.

To describe the relation of the wind to the Rongbuk valley topography, the horizontal wind speed was divided into axial and normal wind speeds according to the valley direction. The positive or negative axial wind represents the southerly or northerly (i.e., down- or up-valley wind), and the positive or negative normal wind represents the westerly or easterly.

3. Evolution of the South Asian summer monsoon

3.1 The SASM evolution in 2006

Figure 2 shows the longitude-time sections of zonal wind (U) along 0° – 180° E averaged for 5° – 15° N (Fig. 2a) and meridional wind (V) along 0° – 90° E averaged for 5° S– 5° N (Fig. 2b). The rapid acceleration of the westerly over the North Indian Ocean in late May (approximately Day 140) characterized the onset of the monsoon. Over the course of a few days, the westerly wind intensified with speed greater than 10.0 m s^{-1} and established itself between 45° and 105° E (Fig. 2a), and a southerly accelerated to greater than 10.0 m s^{-1} over the western Indian Ocean (Fig. 2b). After its onset, the monsoon experienced several active periods from late June to mid July, mid to late August, and late September to early October. During these periods, the westerly extended farther eastward to approximately 150° E with wind speed greater than 10.0 m s^{-1} . The break periods of the monsoon occurred in mid June, late July, and early and mid September, which were characterized by lulls in the westerly. These active and break periods of the SASM varied from days to weeks, consistent with previous studies (Webster et al., 1998).

To quantify the SASM evolution, previous studies adopted several indices (Webster and Yang, 1992; Lau and Yang, 1997; Webster et al., 1998; Goswami et al., 1999; Wu and Wang, 2001; Li and Zeng, 2002), and this study uses the Webster and Yang (1992) index (WYI) as a monsoon index to describe the broad-scale variability of the SASM. This index is defined by a time-mean zonal wind (U) shear between 850 and 200 hPa, namely, U_{850} – U_{200} , averaged over the South

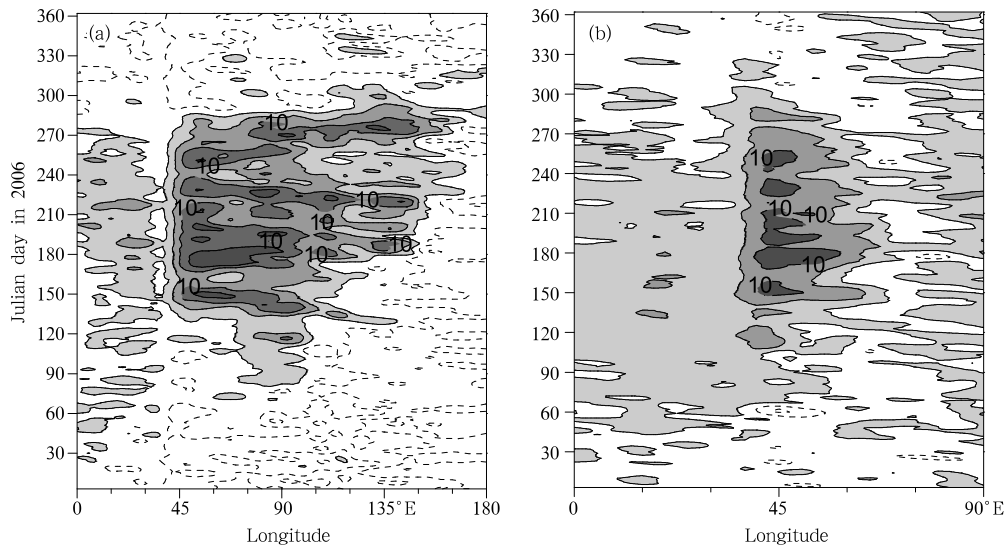


Fig. 2. Longitude-time sections of (a) 850-hPa zonal velocity component (U) along 0° – 180° E, averaged between 5° and 15° N, with the westerly ($U > 0$) shaded, and (b) 850-hPa meridional velocity component (V) along 0° – 90° E, averaged between 5° S and 5° N, with the southerly ($V > 0$) shaded. All data are 5-day running means in m s^{-1} .

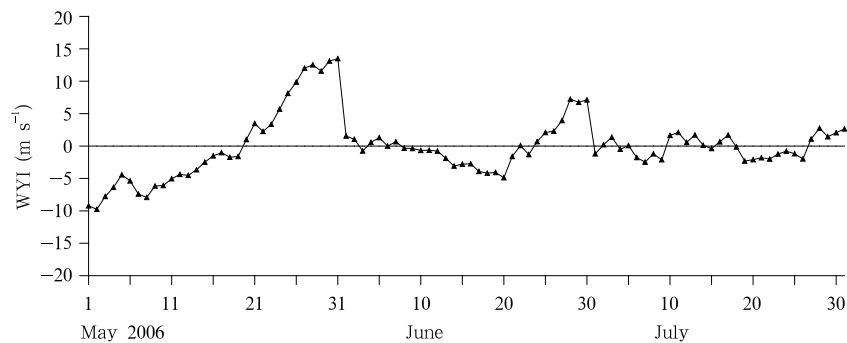


Fig. 3. Variation of the SASM index from May to July 2006, after Webster and Yang (1992).

Asian region (0° – 20° N, 40° – 110° E) (Fig. 3). The WYI increased to a positive value from mid May and maintained large values from 26 to 31 May during the onset of the SASM. The WYI showed a small variation of $\pm 1 \text{ m s}^{-1}$ from 1 to 12 June, which was related to the unsteady monsoon variation. It maintained a large negative value from 13 to 21 June, experienced a two-day transfer from 22 to 23 June, and increased to a large positive value from 24 to 30 June. The averaged values were -3.2 and 4.3 m s^{-1} for 13–21 and 24–30 June, respectively, and they were characterized as one break and one active period during the HEST2006

campaign.

3.2 Synoptic situations over the South Asian region

The SASM experienced one break and one active period during the HEST2006 campaign, and the coinciding synoptic situations over the South Asian region should be different between them. Figure 4 shows the 500-hPa geopotential height field, averaged for the whole campaign period (Fig. 4a) and the break (Fig. 4b) and active (Fig. 4c) SASM periods. During the entire campaign (Fig. 4a), a weak low pressure con-

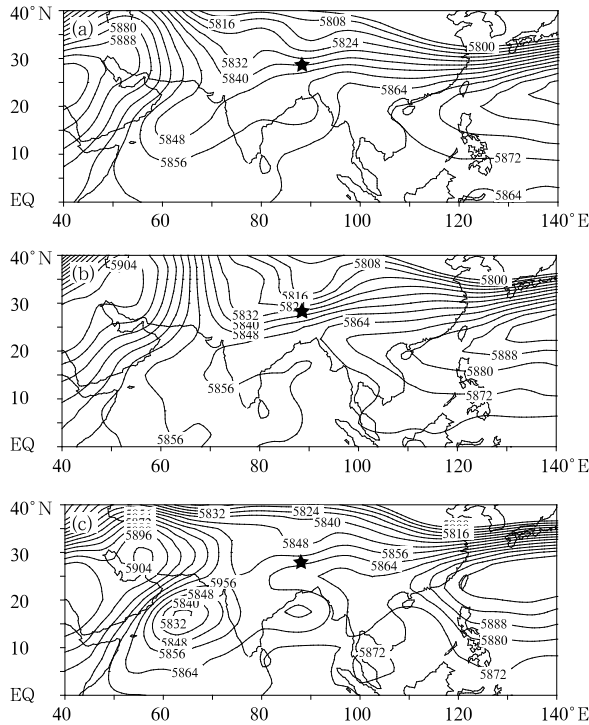


Fig. 4. Horizontal distributions of geopotential height at 500 hPa during (a) the campaign, (b) SASM break, and (c) SASM active periods, with a contour interval of 4 m. The star denotes the observation region.

trolled most of the TP and extended southwest to the Arabian Sea. During the break period (Fig. 4b), the TP low pressure in Fig. 4a became stronger, with strong westerly dominating the observation region. But during the active period (Fig. 4c), the low pressure system in Fig. 4a moved to the north of the plateau, and a strong low appeared over the Arabian Sea with a centered geopotential height value lower than 5832 m. This low extended eastward to the Bay of Bengal and formed a second low pressure there. During this period, the observation region was controlled by both the southwesterly from the Bay of Bengal and the westerly from the TP low.

Affected by the synoptic situations, the thermal, moisture, and convective conditions over the South Asian region may also be different between the SASM break and active periods. Figure 5 shows the air temperature distributions at 500 hPa for the campaign period, the break, and the active SASM periods over the South Asian region. During the campaign (Fig. 5a), the temperature exceeded 270.0 K over the

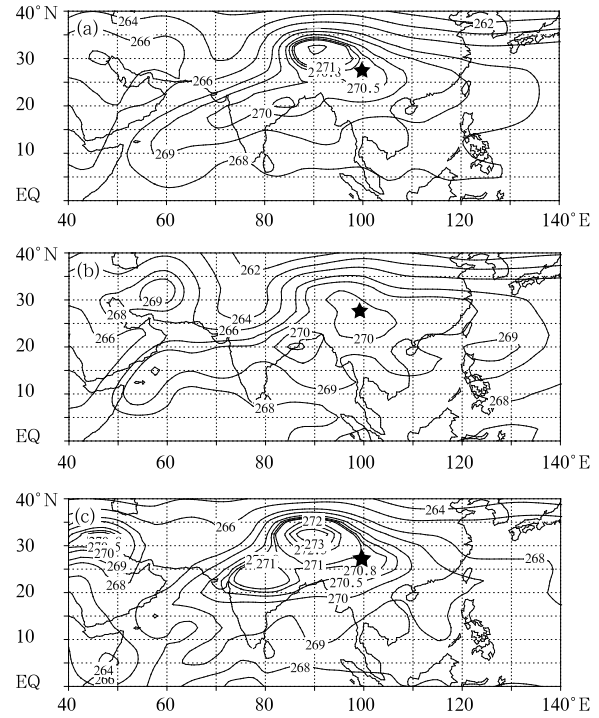


Fig. 5. Horizontal distributions of temperature at 500 hPa during (a) the campaign, (b) SASM break, and (c) SASM active periods. The star denotes the observation region.

eastern TP and exhibited a maximum value of 271.5 K at 32.5°N, 90°E. This high temperature over the eastern TP region in Fig. 5a weakened somewhat during the SASM break period (Fig. 5b) and became much stronger during the active period (Fig. 5c). During the same active period, the maximum temperature center remained at the same location as that in Fig. 5a, but with a higher central value of more than 273.5 K. A second high temperature appeared over the northern Indian region. Figure 6 presents the specific humidity distributions at 500 hPa for the three periods. The maximum specific humidity occurred over the eastern TP with maximum values larger than 5.0, 4.5, and 6.0 g kg⁻¹ during the campaign, break, and active periods, respectively. The moisture was much greater over the Arabian Sea and the Bay of Bengal during the active period than during the break period. Figure 7 shows the distributions of precipitation at the three periods related to the convection conditions. During the campaign (Fig. 7a), the east-west oriented precipitation belt was located within 10°–15°N over

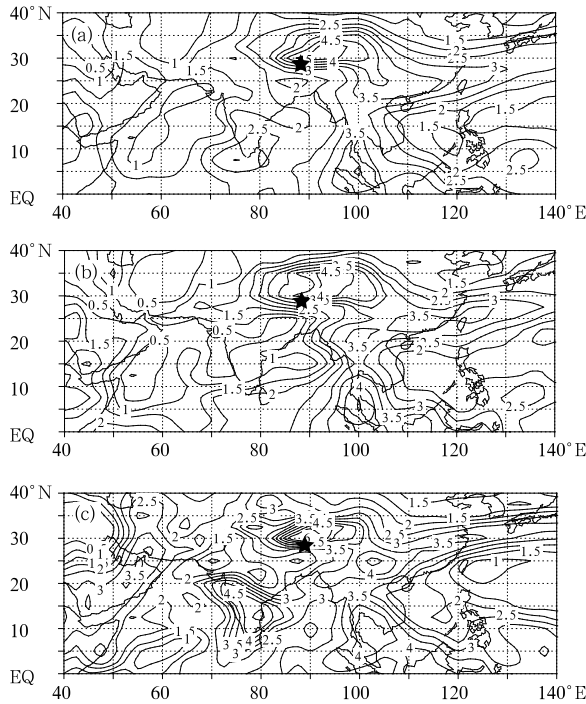


Fig. 6. Horizontal distributions of specific humidity (g kg^{-1}) during (a) the campaign, (b) SASM break, and (c) SASM active periods, with a contour interval of 3.0 g kg^{-1} .

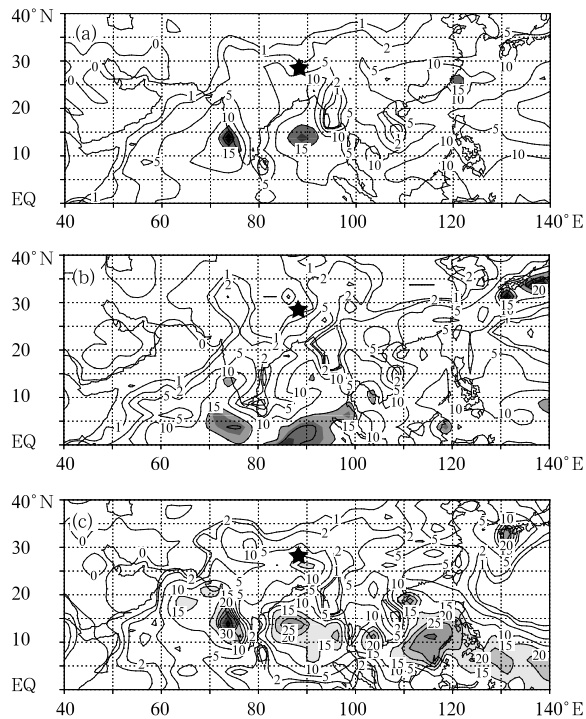


Fig. 7. Horizontal distributions of the pentad-mean precipitation (mm day^{-1}) during (a) the campaign, (b) SASM break, and (c) SASM active periods, with values larger than 50 mm day^{-1} shaded.

the South Asian region, displaying two maxima over the Arabian Sea and the Bay of Bengal but with the maximum values less than 25.0 mm day^{-1} . During the SASM break period (Fig. 7b), the east-west oriented precipitation belt in Fig. 5a moved to south of 10°N , and the two maximum precipitation centers were located at approximately 5°N . During the SASM active period (Fig. 7c), the precipitation belt extended northward to approximately 20°N , and maximum precipitation amounts were greater than 30.0 mm day^{-1} over the Arabian Sea and the Bay of Bengal. In sum, the synoptic situations and the thermal, moisture, and convective conditions over the South Asian region display large differences between the SASM break and active periods.

4. Local atmospheric properties in the Himalayas related to the SASM evolution

The different synoptic situations over the South Asian region illustrate the different thermal, moisture, and convection conditions observed between the SASM break and active periods. For example, the strong westerly in Fig. 4b brought cold and dry air from the Eurasian continent to the observation region and caused temperature to fall (Fig. 5b) and moisture to decrease (Fig. 6b). The lower precipitation rate (Fig. 7b) over the observation region suggests weak convection and clear days. During the SASM active period, however, the strong southwesterly from the Bay of Bengal brought the warm and wet oceanic air to the observation region, increased temperatures (Fig. 5c) and moisture (Fig. 6c) there. The greater amount of precipitation (Fig. 7c) suggests strong convection and more cloudy days over the observation region. The different synoptic situations, thermal, moisture, and convection conditions over the observation region influence the observed atmospheric properties in the Himalayas, and in the following sections, those properties, including the radiative, thermal, and moisture conditions and winds are described during the campaign, SASM break, and active periods.

4.1 Radiation conditions

Figure 8a shows the diurnal variations of the global and net radiation fluxes, averaged for the

campaign, SASM break, and SASM active periods. During the campaign period, the global radiation flux displayed a sine-like variation that increased from approximately 0500 LT (local time), reached a maximum of 984.2 W m^{-2} at 1110 LT and a second maximum of 974.2 W m^{-2} at 1200 LT, and then decreased to 0 at approximately 1900 LT. The net radiation flux displayed a similar diurnal cycle to that of the global radiation flux, with a net heating (positive net radiation flux) from approximately 0700 to 1800 LT and a net cooling (negative net radiation flux) for the rest of the time. The maximum net heating (478.3 W m^{-2}) and net cooling (-72.0 W m^{-2}) occurred at 1110 and 1920 LT, respectively. The global and net radiation fluxes during the SASM break period showed similar diurnal cycles as those during the campaign period, but with the maximum values of 1107.2 and 533.6 W m^{-2} for the global and net radiation fluxes, respectively. During the SASM active period, however, after reaching the maximum of 893.4 and 464.1 W m^{-2} at approximately 1100 LT, the global and net radiation fluxes rapidly decreased along multi-teeth curves. The amplitudes of the global and net radiation fluxes were 984.2 and 550.3 W m^{-2} for the campaign period, 1107.2 and 615.6 W m^{-2} for the SASM break period, and 893.4 and 524.5 W m^{-2} for the SASM active period. The large difference of radiation conditions between the SASM break and active periods is mainly caused by the weather conditions. The weather records showed that 8 days were clear with fewer than 20% cloud amounts during the SASM break period (totally 9 days), and 6 days were cloudy with more than 70% cloud amounts during the SASM active period (totally 7 days). The dominant clear and cloudy days correspond to the weak and strong convections during the SASM break and active periods in Figs. 7b and 7c, respectively, which further indicates the strong and weak solar irradiances. The multi-teeth radiation curves during the SASM active period were also due to the cloud-cover effects.

4.2 Thermal and moisture conditions

Figure 8b shows the diurnal cycles of the soil and surface air temperatures during the three periods. During the campaign period, the soil temper-

ature varied consistently with the global radiation flux with approximately 1 h lags, increasing from the minimum $1.1 \text{ }^{\circ}\text{C}$ at 0510 LT to the maximum $36.8 \text{ }^{\circ}\text{C}$ at 1240 LT, with an amplitude of $35.7 \text{ }^{\circ}\text{C}$. The soil temperature exhibited a diurnal variation during the SASM break/active period similar to that of the campaign period, but with a larger/smaller amplitude of $41.2 \text{ }^{\circ}\text{C}/33.3 \text{ }^{\circ}\text{C}$, which was primarily caused by the strong/weak solar radiation condition. During the campaign period, the surface air temperature increased from the minimum value of $1.0 \text{ }^{\circ}\text{C}$ at 0550 LT to the maximum value of $11.9 \text{ }^{\circ}\text{C}$ at 1350 LT, with an amplitude of $10.9 \text{ }^{\circ}\text{C}$. The surface air temperature was lower during the SASM break period than the SASM active period, due to the much lower tropospheric temperature (see Figs. 5b and 5c) and stronger downward wind flow transport (see Section 4.3) during the break period than during the active period. The specific humidity in Fig. 8c varied in a small range, with low values occurring in the afternoon. The specific humidity during the SASM break period was smaller than during the active period, due to the stronger downward wind flow transport (see Section 4.3) of less moisture from the lower troposphere (see Figs. 6b and 6c) to the surface during the respective periods.

4.3 Winds

Figure 9 shows the diurnal cycles of the axial wind from the surface to 6500 m (the top of the valley) during the campaign, break, and active periods. During the campaign period (Fig. 9a), a weak up-valley wind (negative value) appeared from approximately 0200 to 1000 LT at surface and extended upward to 5400 m. From approximately 1000 to 0200 LT, a down-valley wind (positive value) prevailed in the whole valley, with two maximum values of 12.8 and 12.5 m s^{-1} occurring at 1600 and 1930 LT at 5150 m, respectively. The strong afternoon down-valley wind in the Rongbuk valley is mainly driven by the local thermal forcing due to the snow-ice cover over the Mt. Qomolangma (Zou et al., 2008). The axial wind showed a similar diurnal cycle during the SASM break/active period as that in Fig. 9a, but with strengthened/weakened wind speed. For example, the two maximum down-valley wind speeds in Fig. 9a were strengthened to

16.9 and 16.2 m s^{-1} during the SASM break period (Fig. 9b), and weakened to approximately 10.0 m s^{-1} during the SASM active period (Fig. 9c). The strengthened/weakened axial wind was caused primarily by the stronger/weaker solar radiation during the

SASM break/active period as in Fig. 8a. Figure 10 shows the diurnal cycles of normal wind in the Rongbuk valley during the three study periods. During the campaign (Fig. 10a), the westerly (positive value) persisted for nearly the whole day, except for the easterly

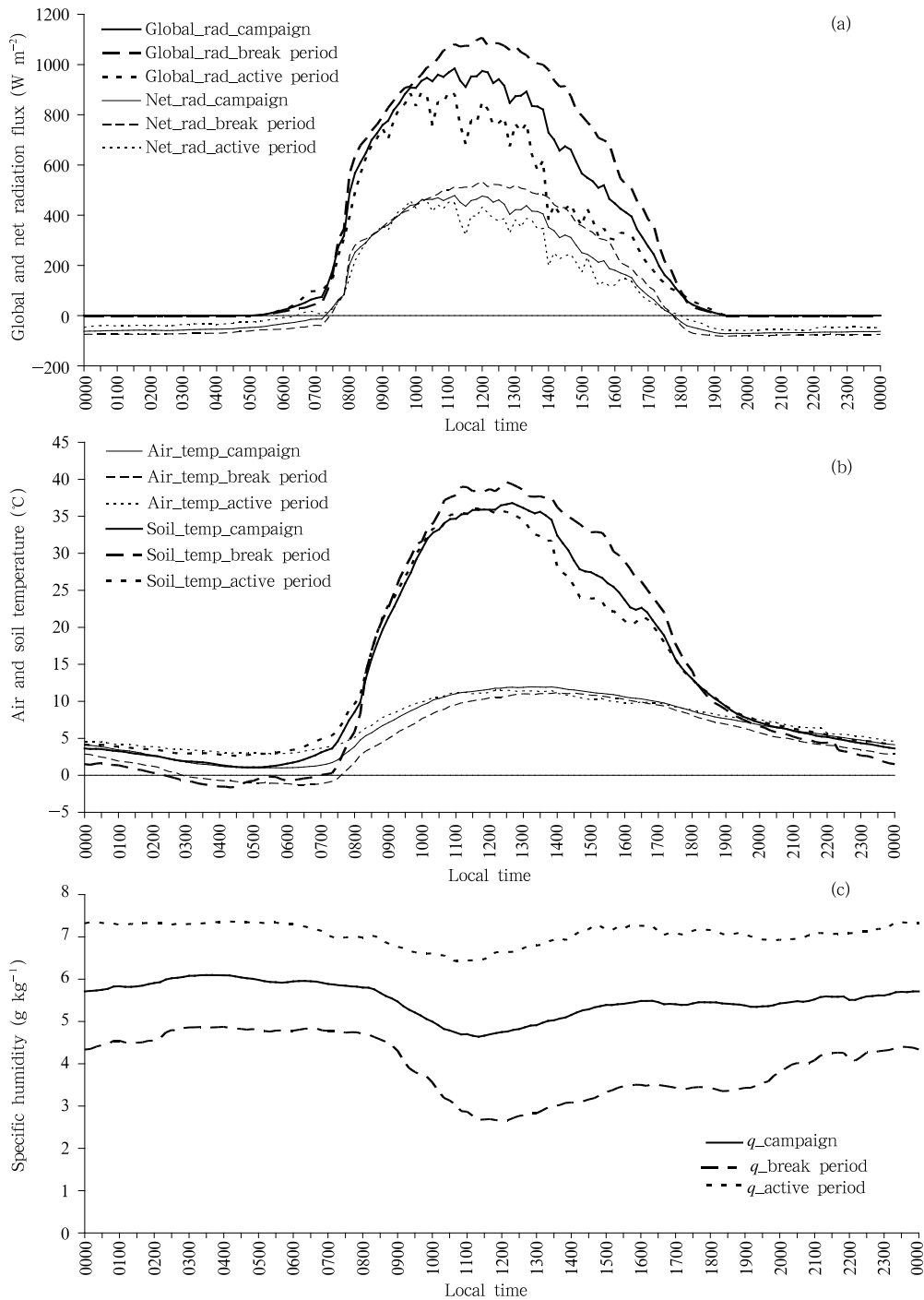


Fig. 8. Diurnal variations of the global and net radiation fluxes (a), soil and surface air temperatures (b), and specific humidity (c) during the campaign, SASM break, and SASM active periods.

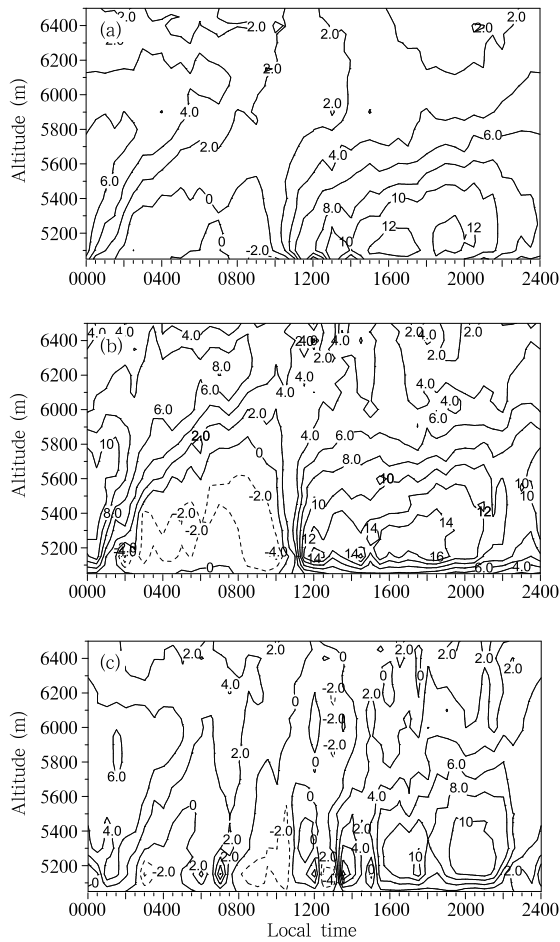


Fig. 9. Diurnal cycles of the axial wind from the valley surface to sub-valley height (6500 m) during (a) the campaign, (b) SASM break, and (c) SASM active periods. The contour interval is 2.0 m s^{-1} , with negative values dashed.

in the morning. The diurnal cycle of normal wind was similar to that of the axial wind, but with a smaller amplitude, due to a branch valley running east from the western Jiuda glacier. The normal wind in the afternoon is strengthened/weakened during the SASM break/active period due to the strong/weak solar radiation condition.

5. Conclusions

The HEST2006 observational campaign was conducted in the Rongbuk valley on the northern slope of Mt. Qomolangma from 1 to 30 June 2006. The meteorological parameters, including the radiation, temperature, moisture, and wind, were continuously observed within the SASM active and break periods.

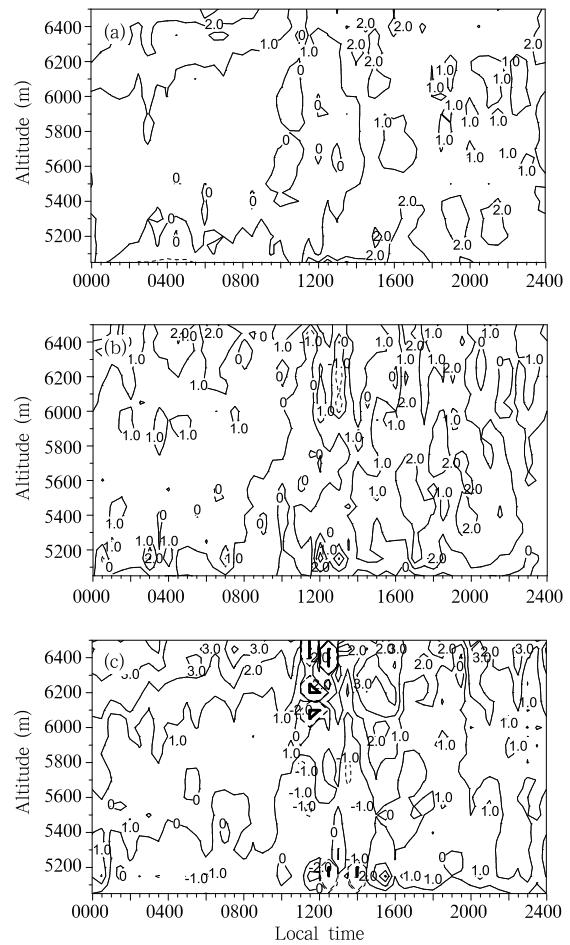


Fig. 10. Diurnal cycles of the normal wind from the valley surface to sub-valley height (6500 m) during (a) the campaign, (b) SASM break, and (c) SASM active periods. The contour interval is 1.0 m s^{-1} , with negative value dashed.

Great differences were found in the synoptic situations over the South Asian region between the SASM active and break periods. For example, the cyclonic vortices were stronger over the Arabian Sea and the Bay of Bengal, with larger amounts of precipitation and higher moisture conditions in the SASM active period than in the break period. The different synoptic situations over the South Asian region affected the local atmospheric properties in the Himalayas. For example, the radiation fluxes and temperatures were much lower in the SASM active period than in the break period, while the specific humidity was much higher in those respective periods. Further discussion suggests that the SASM evolution greatly affects Himalayan atmospheric properties through modified radiation

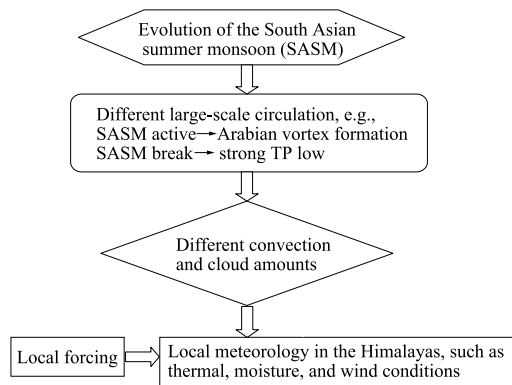


Fig. 11. Sketch map of possible impacts of the South Asian summer monsoon on the local meteorology in the Himalayas.

conditions by the cloud amounts in different synoptic situations. During the SASM active period, the strong cyclonic vortices over the Arabian Sea and Bay of Bengal resulted in a strong southerly that brought warm and wet air northward to the observation region. Cloudy weather with strong convection then dominated the observation region, as documented in local weather records. The cloudy weather blocked the solar irradiance and resulted in low radiation flux at the surface that further lowered the soil temperature and the thermally driven winds. During the break monsoon period, however, clear sky dominated the observation region due to the dry and cold air from the strong continental westerly, resulting in the strongest radiation and thermal conditions. The strong solar radiation and thermal conditions further caused the strengthening of the wind speed in the Himalayas (see Fig. 11).

This study provides insight that the SASM greatly affects local meteorology in the Himalayas, and it consequently affects the regional climate and environment of the TP through the surface-to-air exchange processes. Further studies are therefore needed to understand the relationship between the SASM and Tibetan climate systems.

REFERENCES

- Barros, A., and T. Lang, 2003: Monitoring the monsoon in the Himalayas: Observations in central Nepal, June 2001. *Mon. Wea. Rev.*, **131**, 1408–1427.
- Boos, W. R., and Z. Kuang, 2010: Dominant control of the South Asian monsoon by orographic insulation versus plateau heating. *Nature*, **463**, 218–222.
- Chen, L., E. R. Reiter, and Z. Feng, 1985: The atmospheric heat source over the Tibetan Plateau: May–August 1979. *Mon. Wea. Rev.*, **113**, 1771–1790.
- Ding, Y. H., and D. R. Sikka, 2006: Synoptic systems and weather. *The Asian Monsoon*. Bin Wang, Ed., Praxis Publishing Ltd., Chichester, UK, 131–202.
- , and Y. J. Liu, 2006: Predictability of the South China Sea summer monsoon onset. Symposium on Asian Monsoon—Winter MONEX: A Quarter Century and Beyond. Kuala Lumpur, Malaysia, 4–7 April, 2006.
- Egger, J., and Coauthors, 2000: Diurnal winds in the Himalayan Kali Gandaki valley. Part I: Observations. *Mon. Wea. Rev.*, **128**, 1106–1122.
- , and Coauthors, 2002: Diurnal winds in the Himalayan Kali Gandaki valley. Part III: Remotely piloted aircraft soundings. *Mon. Wea. Rev.*, **130**, 2042–2058.
- Flohn, H., 1957: Large-scale aspects of the “summer monsoon” in South and East Asia. *J. Meteor. Soc. Japan*, **75**, 180–186.
- Gao, D., H. Zou, and W. Wang, 1985: Influences of Brahmaputra river water passage on the precipitation. *Mountain Research*, **3**(4), 239–249. (in Chinese)
- Goswami, B. N., V. Krishnamurthy, and H. Annamalai, 1999: A broad-scale circulation index for the inter-annual variability of the Indian summer monsoon. *Quart. J. Roy. Meteor. Soc.*, **125**, 611–633.
- , and P. K. Xavier, 2003: Potential predictability and extended range prediction of Indian summer monsoon breaks. *Geophys. Res. Lett.*, **30**, doi: 10.1029/2003GL017,810.
- , R. S. Ajaya mohan, P. K. Xavier, and D. Sen-gupta, 2003: Clustering of low pressure systems during the Indian summer monsoon by intraseasonal oscillations. *Geophys. Res. Lett.*, **30**, doi: 10.1029/2002GL016,734.
- He, H., J. W. McGinnis, Z. Song, and M. Yanai, 1987: Onset of the Asian monsoon in 1979 and the effect of the Tibetan Plateau. *Mon. Wea. Rev.*, **115**, 1966–1995.
- Hsu, H. H., C. T. Terng, and C. T. Chen, 1999: Evolution of large-scale circulation and heating during the first transition of Asian summer monsoon. *J. Climate*, **12**, 793–810.

- Krishnamurthy, V., and J. Shukla, 2000: Intraseasonal and interannual variability of rainfall over India. *J. Climate*, **13**, 4366–4377.
- Krishnamurti, T. N., and P. Ardanuy, 1980: The 10 to 20 day westward propagating mode and breaks in the monsoon. *Tellus*, **32**, 15–26.
- Lau, K.-M., and S. Yang, 1997: Climatology and interannual variability of the southern Asian summer monsoon. *Adv. Atmos. Sci.*, **14**, 141–162.
- Li, C., and M. Yanai, 1996: The onset and interannual variability of the Asian summer monsoon in relation to land-sea thermal contrast. *J. Climate*, **9**, 358–375.
- Li, J., and Q. C. Zeng, 2002: A unified monsoon index. *Geophys. Res. Lett.*, **29**, 10.1029/2001GL013874.
- Liu, Y. M., J. C. Chan, J. Y. Mao, and G. X. Wu, 2002: The role of Bay of Bengal convection in the onset of the 1998 South China Sea summer monsoon. *Mon. Wea. Rev.*, **130**, 2731–2744.
- Luo, H., and M. Yanai, 1983: The large-scale circulation and heat sources over the Tibetan Plateau and surrounding areas during the early summer of 1979. Part I: Precipitation and kinematic analysis. *Mon. Wea. Rev.*, **111**, 922–944.
- Matsumoto, J., 1997: Withdrawal of the Indian summer monsoon and its relation to the seasonal transition from summer to autumn over East Asia. *Mausaun*, **41**, 196–202.
- Meinke, I., J. Roads, and M. Kanamitsu, 2007: Evaluation of RSM-simulated precipitation during CEOP. *J. Meteor. Soc. Japan*, **85**, 145–166.
- Sato, T., and F. Kimura, 2007: How does the Tibetan Plateau affect the transition of Indian monsoon rainfall? *Mon. Wea. Rev.*, **135**, 2006–2015.
- Tartari, G., G. P. Verza, and L. Bertolani, 1998: Meteorological data at the pyramid observatory laboratory, Khumbu Valley, Sagarmatha National Park, Nepal. *Limnology of High Altitude Lakes in the Mt. Everest Region (Nepal)*, Lami, A., and G. Giussani, Eds., Mem. Ist. Ital. Idrobiol. Dott. Marco de Marchi, **57**, 23–40.
- Ueno, K., K. Toyotsu, L. Bertolani, and G. Tartari, 2008: Stepwise onset of monsoon weather observed in the Nepal Himalaya. *Mon. Wea. Rev.*, **136**, 2507–2522.
- Wang, B., and H. Lin, 2002: Rainy seasons of the Asian-Pacific monsoon. *J. Climate*, **15**, 386–396.
- Webster, P. J., and S. Yang, 1992: Monsoon and ENSO: Selectively interactive systems. *Quart. J. Roy. Meteor. Soc.*, **118**, 877–926.
- , and Coauthors, 1998: Monsoons: Processes, predictability, and the prospects for prediction. *J. Geophys. Res.*, **103**, 14451–14510.
- Wu, G. X., and Y. Zhang, 1998: Tibetan Plateau forcing and the timing of the monsoon onset over South Asia and the South China Sea. *Mon. Wea. Rev.*, **126**, 913–927.
- Wu, R., and B. Wang, 2001: Multi-stage onset of the summer monsoon over the western North Pacific. *Climate Dyn.*, **17**, 277–289.
- Yanai, M., C. Li, and Z. Song, 1992: Seasonal heating of the Tibetan Plateau and its effects on the evolution of the Asian summer monsoon. *J. Meteor. Soc. Japan*, **70**, 319–351.
- , and C. Li, 1994: Mechanism of heating and the boundary layer over the Tibetan Plateau. *Mon. Wea. Rev.*, **122**, 305–323.
- , and G. X. Wu, 2006: Effects of the Tibetan Plateau. *The Asian Monsoon*. Bin Wang, Ed., Praxing Publishing Ltd., UK, 513–549.
- Yao, T. D., H. Zhou, and X. X. Yang, 2009: Indian monsoon influences altitude effect of $\delta^{18}\text{O}$ in precipitation/river water on the Tibetan Plateau. *Chinese Sci. Bull.*, **54**, 2724–2731, doi: 10.1007/s11434-009-0497-4.
- Ye Duzheng and Gao Youxi, 1979: *Meteorology of the Tibetan Plateau*. Scientific Press, Beijing, 213 pp. (in Chinese)
- Ye, T. Z., 1981: Some characteristics of the summer circulation over the Qinghai-Xizang (Tibet) Plateau and its neighborhood. *Bull. Amer. Meteor. Soc.*, **62**, 14–19.
- Zhang, Z., J. C. Chan, and Y. Ding, 2004: Characteristics, evolution and mechanisms of the summer monsoon onset over Southeast Asia. *Int. J. Climatol.*, **24**, 1461–1482.
- Zou, H., and Coauthors, 2008, Local wind system in the Rongbuk valley on the northern slope of Mt. Everest. *Geophys. Res. Lett.*, **35**, L13813, doi: 10.1029/2008GL033466.